

Process Based Modeling of Total Longshore Sediment Transport

Kevin A. Haas[†] and Daniel M. Hanes[‡]

[†]Georgia Tech Savannah
210 Technology Circle
Savannah, GA 31407, U.S.A.
kevin.haas@gtrep.gatech.edu

[‡]Civil and Coastal
Engineering Department
University of Florida
Gainesville, FL 32611 and
Pacific Science Center
Coastal and Marine Geology
Program, USGS
400 Natural Bridges Drive
Santa Cruz, CA 95060, U.S.A.
dhanes@usgs.gov

ABSTRACT

HAAS, K.A. and HANES, D.M., 2004. Process based modeling of total longshore sediment transport. *Journal of Coastal Research*, 20(3), 853–861. West Palm Beach (Florida), ISSN 0749-0208.



Waves, currents, and longshore sand transport are calculated locally as a function of position in the nearshore region using process based numerical models. The resultant longshore sand transport is then integrated across the nearshore to provide predictions of the total longshore transport of sand due to waves and longshore currents. Model results are in close agreement with the I_r - P_1 correlation described by Komar and Inman (1970) and the CERC (1984) formula. Model results also indicate that the proportionality constant in the I_r - P_1 formula depends weakly upon the sediment size, the shape of the beach profile, and the particular local sediment flux formula that is employed. Model results indicate that the various effects and influences of sediment size tend to cancel out, resulting in little overall dependence on sediment size.

ADDITIONAL INDEX WORDS: *Waves, currents, sediment transport, coastal evolution, numerical models.*

INTRODUCTION

One of the most challenging problems currently attracting considerable effort in the coastal engineering and nearshore processes communities is the prediction of waves, currents, sediment transport, and morphological evolution using numerical models based upon physical principles. In this work we address a very simplified subset of this challenge: the prediction of total longshore sand transport resulting from monochromatic waves incident upon on a two dimensional beach. While this idealized problem is greatly simplified relative to natural phenomenon, it represents an important benchmark in developing the capability to model typically more complex nearshore regions.

One difficulty that arises immediately is that the spatial distribution of the longshore transport of sand on real beaches is a rarely and poorly measured quantity. It is therefore difficult to evaluate the accuracy of predictive models. For example, BAYRAM *et al.* (2001) evaluate local models for longshore sand transport using field measurements obtained at the U.S. Army Corps of Engineers Field Research Facility. As a measure of accuracy, they describe the percent of cases in which the measured values lie within the range of 1/5 to 5 times the model predictions. This rather broad indication of “success” is actually an indication of the large uncertainties

in both field measurements and model predictions. Another example, DAVIES *et al.* (2002), compare several research and practical sand transport models with each other and also to field observations. They find differences of a factor of 10 to 100 to be common, and excellent agreement is considered a factor of two.

The total (gross) longshore transport of sand, I_r , has been measured in the field on many occasions using a variety of measurement techniques (*e.g.*, KOMAR, 1998). While the uncertainties in these measurements are still significant, the body of measurements of total longshore sand transport covers approximately three order of magnitude. As described by KOMAR and INMAN (1970) and the CERC (1984) formula, there is strong evidence that the total longshore transport is related to specific characteristics of the breaking waves. In particular, the product of S_{xy} , the onshore flux of longshore momentum, and C , the wave celerity, both evaluated at the break point, is well correlated with the total longshore sand transport. This product, with the symbol P_1 in Eq (2) below, is sometimes called the longshore (component of) wave power. We regard the I_r - P_1 correlation as perhaps the most reliable feature of longshore sand transport on beaches, and we therefore have chosen to focus our model prediction upon these quantities.

Our approach is to apply models that predict local waves, hydrodynamics, and sediment flux, and from these predic-

tions calculate the total longshore sand transport and the P_1 factor. We regard the ability to reproduce the known I_1 - P_1 correlation as a general verification of the component models. As will be seen, however, the correlation turns out to be so robust that nearly all local sediment transport models we utilized were able to reproduce it adequately, so in the future more detailed verifications will also be required.

Komar and Inman or CERC Formula

The KOMAR and INMAN (1970) or so-called CERC (1984) formula is given as

$$I_1 = KP_1 \quad (1)$$

where I_1 is the immersed-weight sediment transport rate, K is a constant and P_1 is given by

$$P_1 = (ECn \cos \alpha \sin \alpha)_b \quad (2)$$

where E is the wave energy, C is the wave celerity, n is the ratio of wave group speed to wave celerity, α is the wave angle and the subscript b indicates the breakpoint. The volumetric sediment transport rate is given by

$$Q_1 = \frac{I_1}{\rho(s-1)g(1-p)} \quad (3)$$

where ρ is the water density, s is the relative density of the sediment, g is gravity, and p is the porosity of the bed.

The value of the coefficient K has been the subject of much debate. Based upon a variety of measurements KOMAR (1998) suggests a value of 0.70, which is slightly smaller than the value of 0.77 previously suggested by KOMAR and INMAN (1970). In an analysis of existing field data, SCHOONES and THERON (1994) find K to be around 0.4. However, KOMAR (1998) remarks that when the data consisting of suspended load and excluding bed load is dropped from the analysis, the coefficient turns out to be around 0.82. WANG and KRAUS (1999) find K to be in the range of $0.044 < K < 0.541$, albeit with large error bars.

The effect of the grain size upon the value of K has also been examined because the CERC formula contains no other dependence upon grain size. Based on a few field measurements, DEAN and DALRYMPLE (2002) show that K decreases with increasing grain size. This is also shown by KAMPHUIS *et al.* (1986) and DEL VALLE *et al.* (1993). On the other hand, KOMAR (1988) finds no correlation of K with grain size or bed slope, although he remarks that the quality and quantity of data is probably insufficient and there may be counteracting effects of grain size and beach slope.

MODEL FORMULATIONS

This section briefly describes the models which are used in the present study. This includes both the hydrodynamic models as well as the sediment transport models. In addition the methods for calculating shear stresses, bottom friction coefficients and the bathymetry are also described.

Hydrodynamics

The hydrodynamic model system consists of a short-wave transformation component and a short-wave averaged model,

interacting simultaneously to simulate short and long wave motions in nearshore regions. The short-wave model REF/DIF (KIRBY and DALRYMPLE, 1994) is used as the wave driver accounting for the combined effects of bottom induced refraction-diffraction, current induced refraction and wave breaking dissipation. The nearshore circulation model used is SHORECIRC as described in SVENDSEN *et al.* (2002). The model determines the flow pattern by solving the quasi 3-D short-wave averaged hydrodynamic equations.

A Generic Sediment Transport Formula

We first utilize a simple generic local longshore sediment transport relation corresponding to the processes mentioned in the introduction. The time averaged local sediment transport rate is given as

$$q_{HH} = \frac{C_1 f_w}{g} \overline{|\bar{u}|^2} V_{my} \quad (4)$$

with

$$\bar{u}(t) = \bar{u}_w(t) + \bar{V}_b(t) \quad (5)$$

where C_1 is a constant, f_w is the friction factor, g is gravity, V_{my} is the depth averaged longshore current, \bar{u}_w is the near bottom wave orbital velocity, \bar{V}_b is the near bottom current velocity and the overbar represents time-averaging over a short wave period.

Using the definition of the bottom shear stress,

$$\tau = \frac{1}{2} \rho f_w |\bar{u}| \bar{u} \quad (6)$$

equation (4) can be written in terms of the wave-average of the magnitude of the bottom shear stress as follows,

$$q_{HH} = \frac{2C_1}{\rho g} V_{my} \overline{|\tau|} \quad (7)$$

This formula can be interpreted as the product of a sediment load, characterized by the time average bed shear stress magnitude, and an advective velocity, characterized by the depth averaged longshore current velocity. By comparing the model results to be shown later with the value for K (in equation 1) of 0.7 we determined the value of C_1 to be 1.3. This model could be extended by allowing C_1 to vary with sediment characteristics, bedforms or morphology, but such complications are not justified for the present work. Henceforth this model will be referred to as HH.

Bailard, Bowen and Bagnold Formula

A commonly used sediment transport model comes from the energetics approach attributed to BAGNOLD (1966), BOWEN (1980) and BAILARD (1981). The formula for the local immersed-weight longshore transport rate is given as

$$i_{BBB} = \frac{\epsilon_s(1 - \epsilon_b)\rho f_w}{W_o} \overline{|\bar{u}|^3 u_y} + \frac{\epsilon_b \rho f_w}{\tan \phi} \overline{|\bar{u}|^2 u_y} \quad (8)$$

where W_o is the fall velocity, u_y is the longshore component of the instantaneous bottom velocity defined by (5), ϵ_s is the suspended load efficiency factor (typically 0.01), ϵ_b is the bed

load efficiency factor (typically 0.1) and $\tan\phi$ is the angle of internal friction (typically 0.6). This formula includes components of suspended load, the first term, and bed load, the second term. This model will be referred to as BBB.

Watanabe Formula

A sediment transport formula based on the power or energy dissipation concept is used by WATANABE (1992). The rate of longshore sediment transport in this model is defined as

$$q_w = A_c \frac{|\tau_b^{\max} - \tau_{cr}|}{\rho g} V_{my} \tag{9}$$

where A_c is a constant taken to be 2.0, τ_b^{\max} is the maximum instantaneous bottom shear stress for the combined wave and current flow and τ_{cr} is the critical bottom shear stress for the onset of sediment motion based upon the critical Shields parameter. This model is quite similar to the HH model with the main difference being the use of the maximum bottom shear stress rather than the wave-time average of the magnitude of the bottom shear stress. This model will be referred to as W.

Ribberink Formula

A bedload sheet-flow model by RIBBERINK (1998) relates the transport to the effective shear stress. This wave-averaged longshore transport is given as

$$q_R = m \sqrt{(s - 1)gd_{50}^3} \frac{|\theta'| - \theta_{cr} \theta_y / |\theta'|}{|\theta'|} \tag{10}$$

with

$$|\theta'| = \frac{|\tau|}{\rho(s - 1)gd_{50}} \quad \text{and} \tag{11}$$

$$\theta_y = \frac{\tau_y}{\rho(s - 1)gd_{50}} \tag{12}$$

where d_{50} is the median grain size and m and n are constant coefficients equal to 11 and 1.65 respectively. This model will be referred to as R.

Friction Factor

The calculation of the shear stress acting upon the bed is sensitive to the value of the friction factor. Because of the uncertainty involved in determining the friction factor, it is estimated using two different methods. Model runs are done using both friction factors. The first method uses the formula from SWART (1974) to estimate the friction factor f_w^s

$$f_w^s = \exp \left[5.213 \left(\frac{r}{a_o} \right)^{0.191} - 5.977 \right] \tag{13}$$

where a_o is the amplitude of the bottom orbital excursion. The bottom roughness, r , in this formulation is taken to be $2.5 d_{50}$. This friction factor varies with the wave conditions in the cross-shore direction. The second method comes from NIELSEN (1992). The bottom roughness is assumed to be due to bedload transport, and is calculated by using

$$r = 170d_{50} \sqrt{\theta_{2.5} - 0.05} \tag{14}$$

where $\theta_{2.5}$ is determined by

$$\theta_{2.5} = \frac{0.5 f_w^s (a_o \omega)^2}{(s - 1)gd_{50}} \tag{15}$$

ω is the wave frequency and f_w^s is the bottom friction factor determined using the Swart formula with a roughness of $2.5 d_{50}$. The difference between the two methods for determining the friction factor is in the bottom roughness. The method by NIELSEN (1992) results in a bottom roughness nearly 100 times larger than d_{50} , resulting in a much larger friction factor.

Bathymetry

Two types of bathymetry are used in this study: 1) a typical cross-shore profile shape we will refer to as the average beach profile (ABP), and 2) a plane beach. The depth for the ABP is given by the expression

$$h = Ax^{2.3} + 0.05 \text{ m} \tag{16}$$

where x is the cross-shore distance from the shoreline and A is taken from DEAN and DALRYMPLE (2002) based on the sediment size. In order to avoid numerical singularities at the shoreline, we specify a minimum depth of 5 cm which has a negligible effect upon the results.

The slopes of the plane beaches are 1/40, 1/20 and 1/10. These slopes roughly correspond to the ABP by using the distance from the shoreline to the 1 m depth contour. This results in a plane beach slope equal to approximately $A^{3/2}$

RESULTS

A matrix of model runs were conducted using a variety of input conditions: the breaking wave heights were 0.25, 0.5, 1, 1.5, 2, 2.5 and 3 m, the breaking wave angles were 3, 6, 9, 12 and 15 degrees and the wave period was 10 s. Additional tests with wave periods of 6 and 8 s were also performed but will not be presented here because the results were similar. Three grain sizes (d_{50}) were also used: 0.2, 0.4 and 0.8 mm for both types of beach profiles and both friction factors. This resulted in a total of 420 simulations.

The cross-shore depth profile is a function of the grain size through the parameter A in Eq (16). Figure 1 shows the cross-shore profiles for the plane and ABP's for the three sediment sizes. The beach clearly becomes steeper with the larger sediment size. The model domain is longshore uniform, and the cross-shore extent is sufficient to fully resolve the longshore transport for the largest wave conditions.

First, the hydrodynamics are calculated for all combinations of parameters and then the local longshore sediment transport is calculated at each cross-shore grid point (with a grid spacing of 1 m) using each of the four transport equations. Figures 2 and 3 show the cross-shore variation of the wave height, longshore current, and longshore sediment transport for the same case on the ABP and plane beach, respectively. The hydrodynamic conditions are virtually identical on the two types of beaches. The resulting longshore sediment transports are also quite similar.

The total longshore sediment transport is found by integrating across the cross-shore. Figure 4 shows a log-log plot of the total longshore transport on the ABP as a function of

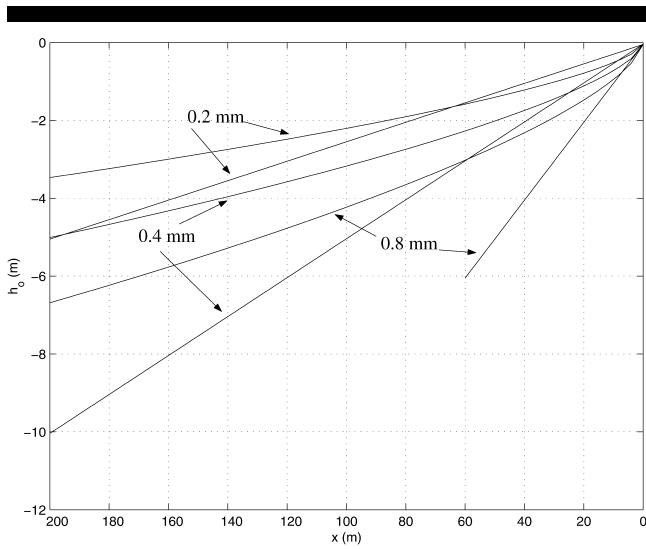


Figure 1. Cross-shore profiles of the plane and ABP for the 3 grain sizes.

P_i , Eq. (2), for the case with $d_{50} = 0.2$ mm using the HH transport equation. The circles represent a number of field and laboratory measurements, as summarized by KOMAR (1998), the x's are the results using the model, and the dark line is the CERC formula with $K = 0.7$. The model results closely reproduce the CERC formula.

Using the HH model as an example we define the ratio R as

$$R = \frac{K_{HH}P_i}{I_{HH}} \quad (17)$$

where K_{HH} is the best fit for K in (1) for the HH model, and I_{HH} is the immersed weight sediment flux calculated by the

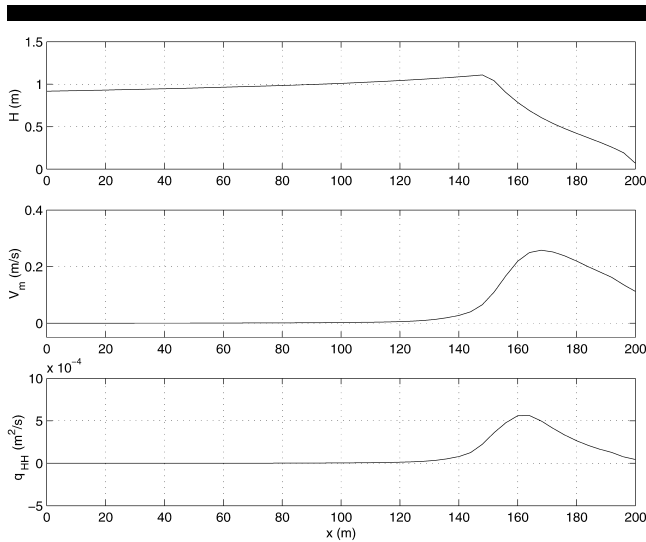


Figure 2. Cross-shore profiles wave height, longshore current and longshore transport for the case on the ABP with 1 m wave height, 3 degree wave angle and 0.2 mm grain size using the HH transport formula and the larger friction factor, Eq (14).

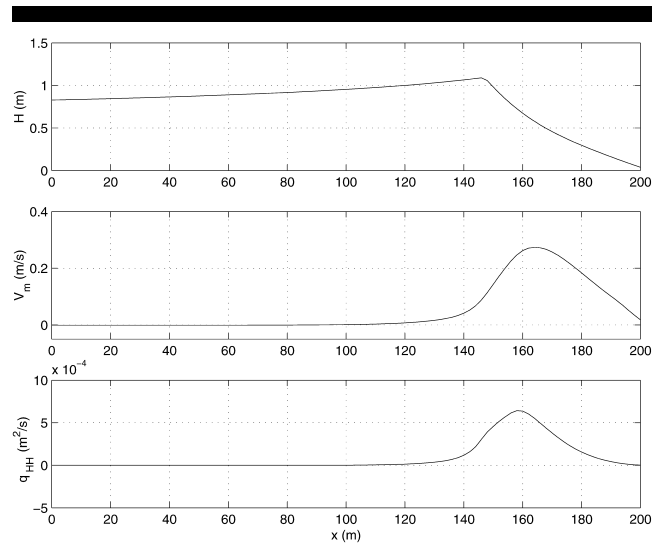


Figure 3. Cross-shore profiles wave height, longshore current and longshore transport for the case on the plane beach with 1 m wave height, 3 degree wave angle and 0.2 mm grain size using the HH transport formula and the larger friction factor, Eq (14).

HH model. The deviations from 1.0 of this ratio are minimized using a least squares method in order to find the best fit K_{HH} . This method allows us to fit a straight line to the log-log plot of Q vs P_i . The line with the best fit K_{HH} is shown in Figure 4 as the light line, which is difficult to distinguish from the dark line (CERC). In this case the best fit K is 0.71, virtually identical to the value for K suggested by KOMAR (1998). The measured data have a large amount of scatter, far larger in fact than the model results. The scatter of the model results is quantified by the variance of the ratio R for

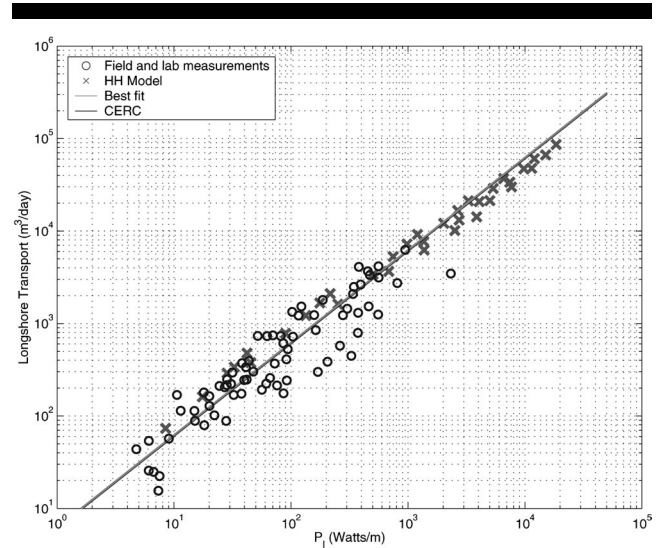


Figure 4. Total longshore transport on the ABP versus wave power using the HH transport formula and the larger friction factor, Eq (14), for $d = 0.2$ mm.

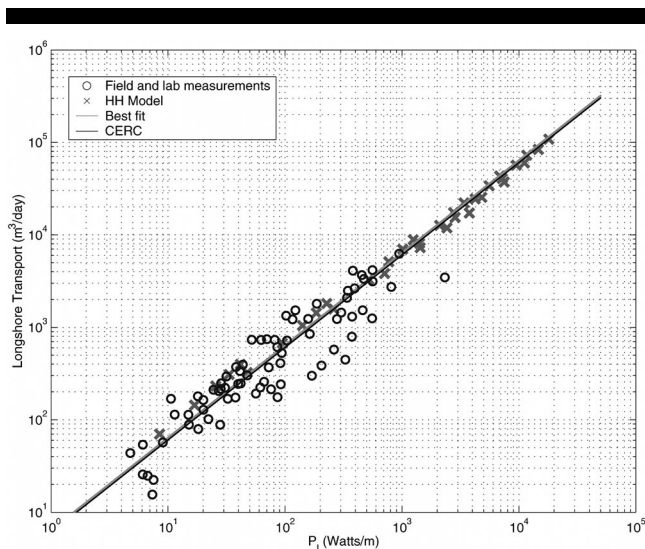


Figure 5. Total longshore transport on the plane beach versus wave power using the HH transport formula and the larger friction factor, Eq (14), for $d = 0.2$ mm.

the 35 simulations for each grain size. In this case the variance of R is 0.11.

Figure 5 is for the same case as Figure 4, but on the plane beach. The best fit K in this case is 0.73 and the variance is 0.034. The primary difference between the plane and ABP model results is that there is slightly more scatter on the ABP.

Next, the local sediment transport is calculated using each of the other predictive formulae following the same procedures. They all result in plots similar to Figures 4 and 5, but with different values of the predicted K and different amounts of scatter. In order to facilitate the analysis, the K values calculated from all the model runs with the ABP beach are tabulated in Table 1 and with the plane beach in Table 3. The scatter (R variance) of the results from the models with the ABP beaches are documented in Table 2 and with the plane beaches in Table 4.

In general the larger friction factor, Eq (14), results in larger values of K. Also, the larger friction factor produce less scatter in the model results using the HH, W and R transport formulae but only slightly less scatter for the BBB formula.

The W formula tends to give the largest total transport while R gives the least. The other two formulae give total

Table 1. Estimate of K in Eq (1) using each type of transport equation on the ABP.

| f_w | d_{50} (mm) | Transport Model | | | |
|---------------|---------------|-----------------|------|------|-------|
| | | HH | BBB | W | R |
| Eq 14 (large) | 0.2 | 0.71 | 0.64 | 1.16 | 0.19 |
| | 0.4 | 0.77 | 0.39 | 1.31 | 0.22 |
| | 0.8 | 0.87 | 0.31 | 1.57 | 0.28 |
| Eq 13 (small) | 0.2 | 0.56 | 0.49 | 0.75 | 0.081 |
| | 0.4 | 0.67 | 0.34 | 0.90 | 0.10 |
| | 0.8 | 0.81 | 0.30 | 1.15 | 0.13 |

Table 2. Variance of the ratio R, Eq (18) for each type of transport equation on the ABP. Larger values represent increased scatter in the model results.

| f_w | d_{50} (mm) | Transport Model | | | |
|---------------|---------------|-----------------|-------|-------|-------|
| | | HH | BBB | W | R |
| Eq 14 (large) | 0.2 | 0.11 | 0.040 | 0.067 | 0.075 |
| | 0.4 | 0.049 | 0.043 | 0.028 | 0.022 |
| | 0.8 | 0.036 | 0.039 | 0.036 | 0.026 |
| Eq 13 (small) | 0.2 | 0.56 | 0.022 | 0.25 | 0.68 |
| | 0.4 | 0.28 | 0.063 | 0.096 | 0.29 |
| | 0.8 | 0.13 | 0.056 | 0.068 | 0.14 |

transports somewhere in between. The sediment transport on the plane beach tends to be larger than on the ABP. All the formulae, except BBB, have constant coefficients which are set to their standard values. These coefficients could be adjusted in which case each could generate values of K to essentially match the CERC formula. Note that the BBB formula has efficiencies which are set to standard values, but are actually quite uncertain in the surfzone.

All of the transport formulae are somewhat sensitive to sediment size. The HH, W and R formulae tend to increase transport with larger sediment while BBB tends to decrease transport with larger sediment size. The scatter of the model results tends to decrease a little with larger sediment sizes, although not consistently. Overall, the sensitivity of the total longshore sediment transport to sediment size is remarkably small. To understand why this is the case, we have to examine all the effects contained in the models which are influenced by the sediment size.

The hydrodynamics, especially the longshore current, is quite sensitive to the grain size through the beach slope and the friction factor, under the assumption that the bed is reasonably flat and bedforms don't contribute significantly to the flow resistance. As the grain size increases so does the beach slope. As the beach gets steeper, the waves break closer to the shoreline. For any given wave condition, the waves break over a shorter distance on a steeper beach. This results in a stronger radiation stress gradient and hence stronger longshore currents.

We isolate the effect of the bottom slope by keeping the bottom roughness constant but varying the slope for a given breaking wave condition. In this case, the radiation stress forcing is significantly larger on the steeper slope because the surf zone width is significantly narrower. The top two panels of Figure 6 show the longshore current and longshore bottom

Table 3. Estimate of K in Eq (1) using each type of transport equation for the plane beach.

| f_w | d_{50} (mm) | Transport Model | | | |
|---------------|---------------|-----------------|------|------|------|
| | | HH | BBB | W | R |
| Eq 14 (large) | 0.2 | 0.73 | 0.68 | 1.20 | 0.20 |
| | 0.4 | 0.86 | 0.46 | 1.51 | 0.26 |
| | 0.8 | 1.0 | 0.41 | 1.97 | 0.36 |
| Eq 13 (small) | 0.2 | 0.64 | 0.59 | 0.84 | 0.10 |
| | 0.4 | 0.82 | 0.45 | 1.13 | 0.14 |
| | 0.8 | 0.93 | 0.40 | 1.15 | 0.17 |

Table 4. Variance of the ratio R Eq (18) for each type of transport equation for the plane beach. Larger values represent increased scatter in the model results.

| f_w | d_{50} (mm) | Transport Model | | | |
|------------------|---------------|-----------------|-------|--------|--------|
| | | HH | BBB | W | R |
| Eq 14 (large) | 0.2 | 0.034 | 0.028 | 0.030 | 0.013 |
| | 0.4 | 0.013 | 0.041 | 0.018 | 0.0081 |
| | 0.8 | 0.010 | 0.014 | 0.0077 | 0.0070 |
| Eq 13 (small) | 0.2 | 0.25 | 0.070 | 0.087 | 0.24 |
| | 0.4 | 0.090 | 0.024 | 0.027 | 0.086 |
| | 0.8 | 0.068 | 0.098 | 0.068 | 0.058 |

shear stress for this case. For the steeper beach the peaks of the current and stress are shifted shoreward and are much larger. This is a direct result of the increased radiation stress forcing. The longshore sediment transport shown in the bottom four panels show a significant increase in transport due to the increase in longshore current as well as the increased shear stress.

Counteracting the increase in radiation stress forcing is an increase in the bottom friction coefficient through an increase

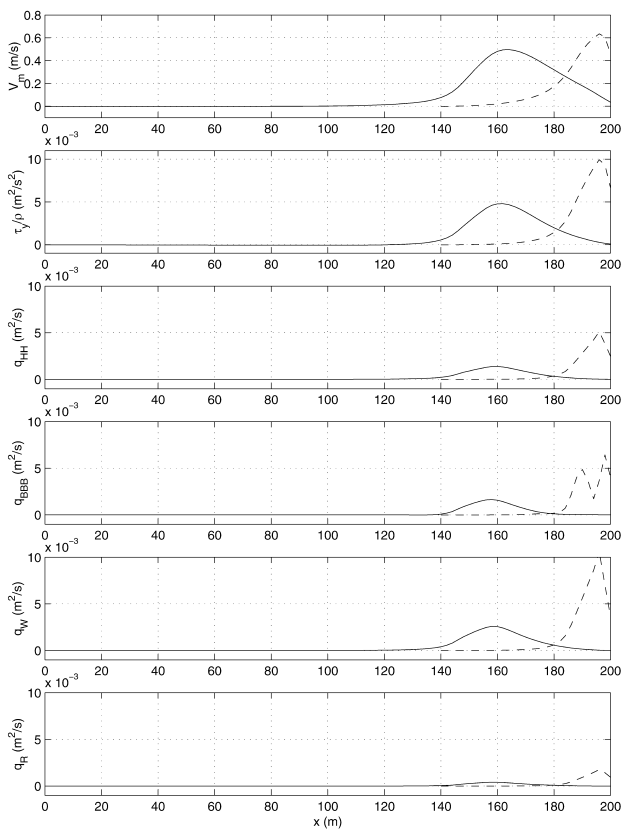


Figure 6. Cross-shore profiles of longshore current, bottom shear stress and longshore transport based on HH, BBB, W and R for $d_{50} = 0.2$ mm (solid) and $d_{50} = 0.8$ mm (dashed) where only the slope varies, but not the friction factor. The case is on the ABP, with a breaking wave height of 1m, a wave angle of 9 degrees and the larger friction factor, Eq (14).

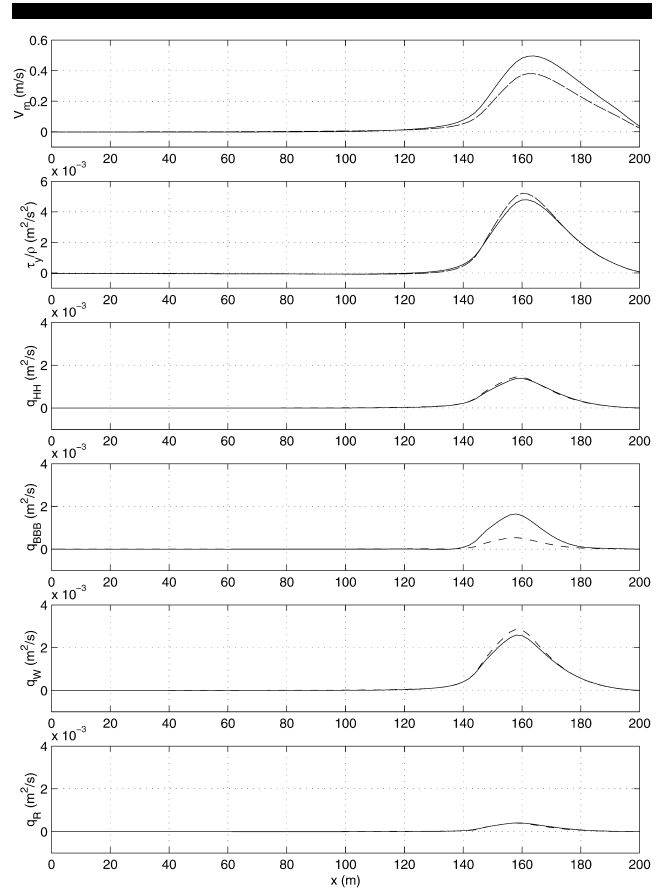


Figure 7. Cross-shore profiles of longshore current, bottom shear stress and longshore transport based on HH, BBB, W and R for $d_{50} = 0.2$ mm (solid) and $d_{50} = 0.8$ mm (dashed) where the slope is constant but the friction factor varies. The case is on the ABP, with a breaking wave height of 1m, a wave angle of 9 degrees and the larger friction factor, Eq (14).

in bottom roughness (due to larger sediment). Isolating the effect of grain size on the longshore sediment transport via the roughness is accomplished by keeping the slope constant but changing the friction factor. Under such a case, the radiation stress forcing will be identical, and hence, ideally the bottom shear stress will be the same since this is the primary momentum balance. However, the longshore current will decrease with the increased roughness because the friction factor is larger.

The upper two panels of Figure 7 show the resulting longshore current and longshore bottom shear stress for these conditions. The longshore current indeed decreases for the larger sediment size. However, the bottom shear stress increases slightly. This is because the momentum balance is not as simple as the ideal situation and the convective and mixing terms are different due to the weaker longshore currents.

The bottom four panels in Figure 7 show the longshore sediment transport based on the four formulae. The decrease in the longshore current decreases transport in all the formulae, however, HH, W and R are based on the shear stress and

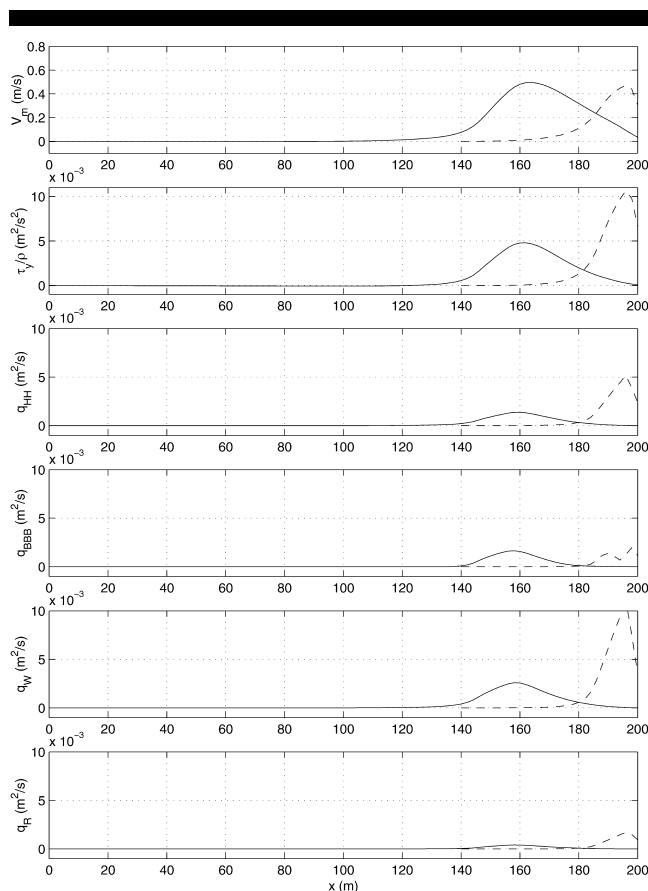


Figure 8. Cross-shore profiles of longshore current, bottom shear stress and longshore transport based on HH, BBB, W and R for $d_{50} = 0.2$ mm (solid) and $d_{50} = 0.8$ mm (dashed). The case is on the ABP, with a breaking wave height of 1m, a wave angle of 9 degrees and the larger friction factor, Eq (14).

hence the transport increases slightly. BBB is highly sensitive to reduction in the longshore current, however, and transport decreases significantly.

The combined effect of the steeper beach and the increased drag on the longshore current is seen in the first panel of Figure 8. Clearly the longshore current extends over a much larger region on the milder sloping beach due to the larger width of the surf zone. However, the magnitude of the peak of longshore current is similar for the two cases. This is because the bottom shear stress shown in the second panel of Figure 8 is much larger due to the increased friction factor resulting from the increased roughness associated with the larger sediment size. The overall effect of grain size is to decrease the total longshore current with increasing grain size, which decreases the total longshore sediment transport.

Looking at each of the longshore sediment transport formulae in detail, we see they are all functions of the grain size. Each of them are a linear function of the friction factor f_w except R, which is a nonlinear function of f_w . As shown earlier, when the friction factor increases corresponding to a

larger grain size, the shear stress increases and each transport formula predicts more longshore transport.

The HH transport formula only has grain size dependence via the shear stress. The variation of the longshore sediment transport using HH for two sediment sizes is shown in the third panel of Figure 8. Even though the magnitude of the peak of the longshore current is similar for the two grain sizes, the magnitude of the peak of the longshore transport is larger for the bigger grain size. The increase in transport due to the increase in bottom shear stress is larger than the decrease due to the hydrodynamics, such that the total transport increases slightly with grain size.

In addition to the friction factor, the BBB formula is also a function of the fall velocity W_o . As the fall velocity increases due to larger grain sizes, the suspended sediment transport decreases. The cross-shore variation of the longshore transport is shown in the fourth panel of Figure 8. With this formula, the longshore transport is clearly decreased for the larger sediment case. The decrease due to the fall velocity and the longshore current is much more prevalent than the increase due to the bottom shear stress.

In W, the critical shear stress τ_{cr} is dependent on the grain size. Therefore, a larger grain size leads to a larger critical shear stress required to initiate grain movement, and therefore slightly less transport. This model is a function of the bottom shear stress and because the longshore currents for the different grain sizes are similar in magnitude, the bottom shear stress is larger due to the bigger friction factor for the larger grain size resulting in more longshore transport. The decrease due to the larger critical shear stress is much less than the increase due to the friction factor resulting in an increase in transport as seen in the fifth panel of Figure 8.

The R formula is dependent on d_{50} directly such that larger grain sizes result in less transport in this formulation. As seen in the bottom panel of Figure 8, the longshore transport decreases with larger grain sizes. This indicates that the direct dependence on the grain size has a smaller effect than the bottom shear stress.

Even though the different transport formulae contain several mechanisms, they result in only a weak dependence (less than 25% variations in K) on the grain size. The reason is that all the models have several mechanisms which cause increases or decreases in transport such that they counteract each other. This is perhaps the reason why the CERC formula works robustly without sediment size dependence.

DISCUSSION

It has often been noted that the I_1 - P_1 correlation is remarkably robust, which is particularly surprising because it does not contain many of the parameters which are expected to be important. In shallow water, the P_1 factor is only sensitive to two factors, the breaking wave height and breaking wave angle. Foremost amongst the “omitted” parameters are the beach slope and sediment size.

Explanations of this apparent deficiency are in part provided by KOMAR (1998), and will be expanded upon here. We base the following upon the simplified model that the sediment is suspended by the bed shear stress and is advected

by the longshore current. The flow is assumed to consist of a cross-shore oscillatory component due to waves and a steady longshore component due to the longshore current: $\bar{u}(t) = u_0 \sin(t)\bar{i} + V_{my}\bar{j}$.

Combining equations 5 and 6 and the assumption stated above, the time average of the magnitude of the bottom shear stress is:

$$\overline{|\tau|} = \frac{1}{2} \rho f_w \sqrt{u_0^2 \sin^2(t) + V_{my}^2} = \frac{1}{2} \rho f_w u_0^2 f_1, \quad (18)$$

where $f_1 = \sqrt{\sin^2(t) + V_{my}^2/u_0^2}$. In the limit of small longshore currents relative to the wave orbital current speed, $f_1 = 2/\pi$.

Using linear long-wave theory and assuming $H/h = \gamma$ we then take $gh\gamma/4$ as the value of u_0^2 in the surf zone such that

$$|\tau| = \frac{1}{8} \rho f_w \gamma^2 gh f_1. \quad (19)$$

For bathymetries with no longshore gradients, the longshore current is related to the gradient in the radiation stress component S_{xy} (e.g., LONGUET-HIGGINS, 1970), given approximately by

$$V_{my} = \frac{5\pi\sqrt{g}\gamma}{8f_w} \left(\frac{\sin \alpha_b}{\sqrt{h_b}} \right) \beta h \quad (20)$$

Here we have assumed a plane beach ($h = \beta x$), a wave breaking criterion $H = \gamma h$, $C = \sqrt{gh}$, and weak longshore currents ($f_1 = 2/\pi$). Using these approximations and the sediment flux formula from equation (7), the local longshore sediment transport is then proportional to

$$i(x) \propto \rho g^{1.5} \gamma^3 \left(\frac{\sin \alpha_b}{\sqrt{h_b}} \right) \beta h^2, \quad (21)$$

where we have omitted dimensionless constants such as porosity and specific density. Integrating across the surf zone yields the total longshore sediment transport

$$I_1 \propto \rho g^{1.5} \gamma^3 \sin(\alpha_b) h_b^{2.5}. \quad (22)$$

Under the same assumptions we find

$$P_1 = (ECn \cos \alpha \sin \alpha)_b = \frac{1}{8} \rho g^{3/2} \gamma^2 h_b^{5/2} n_b \cos \alpha_b \sin \alpha_b. \quad (23)$$

If we assume $n_b \sim 1$, $\cos \alpha_b \sim 1$, then the ratio of these two expressions is proportional only to the factor γ . The success of the I_1 - P_1 correlation (on a log-log plot) implies that the factor γ , the sediment porosity, and the sediment density do not vary by more than an order of magnitude in nature, which is in fact the case. Note that the influence of both the drag coefficient and the beach slope have cancelled in this derivation.

CONCLUSIONS

The well known I_1 - P_1 correlation for the total longshore transport of sand has been reproduced through the use of numerical models that predict the local waves, currents, and sediment flux. Although the proportionality coefficient K was found to vary somewhat depending upon the specific model components, the sediment size, and the shape of the beach

profile, the overall correlation was found to be remarkably robust. When quantifying the effects of grain size on longshore transport, we found that many grain-size related effects counteract each other, resulting in limited overall grain size dependence. Ironically, because all four sediment transport models showed similar skill, these specific results cannot be used to comment on the validity of the particular transport formula.

ACKNOWLEDGMENTS

This work was sponsored by the US Office of Naval Research and the National Science Foundation through the National Oceanographic Partnership Program. KAH was also supported by the U.S. Army Research Office. During the latter stages of this work DMH was supported by the Coastal and Marine Geology Program of the U.S. Geological Survey. Internal reviews by Curt Storlazzi and Peter Ruggiero are appreciated.

LITERATURE CITED

- BAGNOLD, R.A., 1966. An approach to the sediment transport problem from general physics. Professional paper 422-I, US Geological Survey.
- BAILLARD, J.A., 1981. An energetics total load sediment transport model for a plane sloping beach. *Journal of Geophysical Research*, 86, 10938-10954.
- BAYRAM, A.; LARSON, M.; MILLER, H.C., and KRAUS, N.C., 2001. Cross-shore distribution of longshore sediment transport: comparison between predictive formulas and field measurements. *Coastal Engineering*, 44, 79-99.
- BOWEN, A.J., 1980. Simple models of nearshore sedimentation: Beach profiles and longshore bars. In *Coastline of Canada*, pages 1-11, Halifax. Geological Survey of Canada.
- CERC, 1984. *Shore Protection Manual*. Vicksburg, Mississippi: U.S. Army Coastal Engineering Research Center, Corps of Engineers.
- DAVIES, A.G.; VAN RIJN, L.C.; DAMGAARD, J.S.; VAN DE GRAAFF, J., and RIBBERINK, J. S., 2002. Intercomparison of research and practical sand transport models. *Coastal Engineering*, 46, 1-23.
- DEAN, R.G. and DALRYMPLE, R.A., 2002. *Coastal Processes with Engineering Applications*. Cambridge, UK: Cambridge University Press.
- DEL VALLE, R.; MEDINA, R., and LOSADA, M. A., 1993. Dependence of the coefficient K on the grain size. *J. of Waterway, Port, Coastal and Ocean Engineering*, 118, 417-432.
- KAMPHUIS, J.W.; DAVIES, M.H.; NAIRN, R.B., and SAYAO, O.J., 1986. Calculation of littoral sand transport rate. *Coastal Engineering*, 10, 1-21.
- KIRBY, J. and DALRYMPLE, R., 1994. Combined refraction/diffraction model REF/DIF 1, version 2.5. *Technical Report CACR-94-22*, Center for Applied Coastal Research, University of Delaware.
- KOMAR, P., 1988. Environmental controls on littoral sand transport. *Proceedings 21st Coastal Engineering Conference (ASCE)*, pp. 1238-1252.
- KOMAR, P.D., 1998. *Beach Processes and Sedimentation*. Englewood Cliffs, New Jersey: Prentice Hall.
- KOMAR, P.D. and INMAN, D.L., 1970. Longshore sand transport on beaches. *Journal of Geophysical Research*, 75, 5514-5527.
- NIELSEN, P., 1992. *Coastal Bottom Boundary Layers and Sediment Transport*. World Scientific.
- RIBBERINK, J.S., 1998. Bed-load transport for steady flows and unsteady oscillatory flows. *Coastal Engineering*, 34, 59-82.
- SCHOONES, J.S. and THERON, A.K., 1994. Accuracy and applicability of the SPM longshore transport formula. *Proceedings 24th Coastal Engineering Conference (ASCE)*, Volume 3, pp.2595-2609.
- SVENDSEN, I.A.; HAAS, K.A., and ZHAO, Q., 2002. Quasi-3D nearshore

- circulation model SHORECIRC, *Report # 2002-01*, Center for Applied Coastal Research, University of Delaware.
- SWART, D.H., 1974. Offshore sediment transport and equilibrium beach profiles. *Laboratory Publication No. 131*, Delft Hydraulics.
- WANG, P. and KRAUS, N.C., 1999. Longshore sediment transport rate measured by short-term impoundment. *Journal of Waterway, Port, Coastal and Ocean Engineering*, 125, 118–126.
- WATANABE, A., 1992. Total rate and distribution of longshore sand transport. *Proc. 23rd Coastal Engineering Conference (ASCE)*, Volume 3, pp. 2528–2541.